



## UvA-DARE (Digital Academic Repository)

### Cell resolved blood flow modeling with the Lattice Boltzmann method

*Cell deformability and transport in diseases*

Czaja, B.E.

**Publication date**

2020

**Document Version**

Other version

**License**

Other

[Link to publication](#)

**Citation for published version (APA):**

Czaja, B. E. (2020). *Cell resolved blood flow modeling with the Lattice Boltzmann method: Cell deformability and transport in diseases*. [Thesis, fully internal, Universiteit van Amsterdam].

**General rights**

It is not permitted to download or to forward/distribute the text or part of it without the consent of the author(s) and/or copyright holder(s), other than for strictly personal, individual use, unless the work is under an open content license (like Creative Commons).

**Disclaimer/Complaints regulations**

If you believe that digital publication of certain material infringes any of your rights or (privacy) interests, please let the Library know, stating your reasons. In case of a legitimate complaint, the Library will make the material inaccessible and/or remove it from the website. Please Ask the Library: <https://uba.uva.nl/en/contact>, or a letter to: Library of the University of Amsterdam, Secretariat, P.O. Box 19185, 1000 GD Amsterdam, The Netherlands. You will be contacted as soon as possible.

# 5

## A Hierarchical Multiscale Model for Blood Flow

This chapter aims to bring three dimensional cell-resolved blood flow to vessels above a millimeter in diameter. Numerical modeling of the transport and rheology of blood in large scale vessels has only been achieved using continuum models due to the substantial computational overhead. Continuum models for blood flow often include recipes for the shear dependence of viscosity, but implicitly assume a constant hematocrit and therefore that viscosity is independent of hematocrit. The novelty of this work is the development of a three dimensional heterogeneous multiscale model for suspension flow. The proposed multiscale model will solve blood flow on the macroscale using an advection diffusion solver to track the concentrations of cells and the Lattice Boltzmann Method to solve the fluid flow. Viscosity and red blood cell concentrations on the macroscale will be informed by microscale cell-resolved sub-models which solve directly the local dynamic viscosity and red blood cell diffusion.

---

This chapter is based on:

Benjamin Czaja, Gábor Závodszy, and Alfons Hoekstra. A heterogeneous multi-scale model for blood flow. In *International Conference on Computational Science*, pages 403–409. Springer, 2020

Daan van Ingen, Benjamin Czaja, Gábor Závodszy, and Alfons Hoekstra. Lees-edwards boundary conditions within the cell resolved lattice boltzmann framework hemocell. *Under Preparation*, 2020

## 5.1. Introduction

The transport of the cells in whole blood, which travels through the cardiovascular system, is a multiscale process. On the smallest scales ( $\mu\text{m}$ ), are the deformations of the RBC membrane and the corresponding momentum exchange with the suspending blood plasma. The emergent rheology exists on larger scales ( $\mu\text{m}$  to mm, cm), arising from collections of RBCs flowing together resulting in non-Newtonian behavior and cell transport. Examples of the non-Newtonian behavior is the decrease in viscosity with the increase of shear rate, as observed by Chien [33]. This bulk behavior is a result of RBC alignment and subsequent break up of rouleaux structures [41, 42, 266] occurring on the cell level. Contemporary numerical models that adequately resolve the transport and rheological properties of whole blood have large amounts of computational overhead and require high performance computing [146, 267].

In the context of this thesis, the cell-resolved model employed in Chapters 2 and 3 requires a solution to the red blood cell membrane model ( $\approx 4000$  equations per cell), the interpolation of momentum from the cell membrane model to the suspending blood plasma via the immersed boundary method ( $\approx 1000$  computations per cell), and the solution to the Newtonian blood plasma through the Lattice Boltzmann Method. In a typical application of this cell-resolved model [119] simulating a  $100\ \mu\text{m}$  diameter straight vessel of length  $200\ \mu\text{m}$  with a hematocrit of 30% ( $\approx 7000$  cells) for a physical second requires approximately 10 days wall clock time on 250 compute cores. Applying a model of this resolution in vessels on the scale of a millimeter and above, is realistically unfeasible.

Blood flow on scales larger than  $300\ \mu\text{m}$  is then consistently modeled as a continuous fluid, as such continuous blood flow models require less computational overhead because they do not include the individual cell dynamics [231, 268, 269]. Continuous models either assume whole blood as a Newtonian fluid or use a non-Newtonian blood viscosity model to approximate the departure of whole from the Newtonian description. Non-Newtonian models describe the change in blood viscosity with a dependency on shear rate like a power law fluid models [270], the Carreau-Yasuda [271] model, or even additionally accounts for yield stress like the Casson model [272]. In these standard shear thinning models viscosity does not depend on hematocrit, and further implicitly assumes a constant hematocrit throughout the entire vessel domain. Since such models do not include the dynamics of the cells they may incorrectly estimate the transport behaviors which are a result of cell-cell collisions within whole blood suspensions. Given such assumptions continuum models have most likely consistently lead to an invalid description of particle diffusivities within whole blood. The ability for present-day shear thinning models to adequately capture the complex blood flow within tortuous vessels is currently unknown.

In order to capture both the non-Newtonian viscosity change of whole blood along with the proper treatment of the transport of suspended blood cells a multiscale model must be developed to account for both processes on all scales of the cardiovascular system. The intent of the multiscale model presented in this chapter is to simulate the cell nature of flowing blood on spatial scales that are currently un-achievable by contemporary cell-resolved blood flow models. This is primarily in vessels above  $300\ \mu\text{m}$  in diameter. Though this research is focused primarily on the rheology and transport properties

of blood, the heterogeneous multiscale modeling (HMM) technique is chosen as a route of development as it is a more general method for modeling multiscale problems and can accommodate many different models together. A three dimensional HMM model to capture the dynamics of complex fluids is not yet available. The goal of this chapter is to set up a 3D HMM for suspension flow for the first time. Additionally an HMM model can be useful for future development for blood flow as it can incorporate models beyond which strictly solve fluid dynamic problems, and can include bio-chemical processes as well.

## 5.2. HMM Outline

The Heterogeneous Multiscale Method [113] is a modeling technique used to numerically solve multiscale problems by coupling multiple sub-models  $\phi$  together that each solve a component separately, through this combination an overall macromodel  $\Phi$  emerges. Heterogeneous here suggests the problem the model is attempting to solve is multi-physics in nature [114]. This means that the overall model can be comprised of multiple models which solve each physical process separately. The aim of this chapter is to develop an HMM model for blood flow that accurately captures the cell nature of flowing blood on the large scale blood vessels in the body. In general this model will, on the large vessel scales (macroscale), simulate blood as a continuous fluid. The macroscale will be informed by microscale sub-models which directly simulate the cell nature of blood via a three dimensional cell-resolved blood flow solver. Though the model presented in this chapter will be focused on the rheology of whole blood, we believe that by choosing such a modeling framework this HMM model for blood flow can eventually be developed in the future, beyond this thesis, to incorporate the other physiological processes of blood flow as well. Examples additions to the HMM model may be sub-models that simulate the diffusion of chemicals in the blood stream, sub-models detailing the initiation and formation of a platelet aggregate during the formation of a blood clot [273], sub-models simulating blood flow and perfusion in the brain, stent deployment [67] and in stent restenosis sub-models [62], as well as cardiac sub-models [274]. Stitching such separate models together will give rise to an overall HMM that not only resolves the rheology of flowing blood, but also the physiology of whole blood throughout the multiple scales of the cardiovascular system.

The rheology and transport of flowing blood, and thus the initial HMM model for blood flow can be separated into two scales, a macroscale and microscale. A schematic highlighting the different numerical models and physical scales considered in the HMM model is shown in Figure 5.1. We define the macroscale in this model, to model the flow, transport, and rheology of whole blood as a continuous fluid. This is achieved through the coupling of two LBM solvers on the macroscale. The first is a LBM to solve the momentum transport and flow of whole blood, the other is a coupled passive scalar field that will track the transport of RBCs as a continuum using a LBM advection diffusion (AD) solver. The non-Newtonian rheology on the macroscale will be influenced from the motions of RBCs on the micro scale. On the micro scale is the cell-resolved blood flow model HemoCell [91], which will directly simulate RBC deformations, collisions, and therefore the resulting cell diffusion and bulk viscosity. This model would be suitable

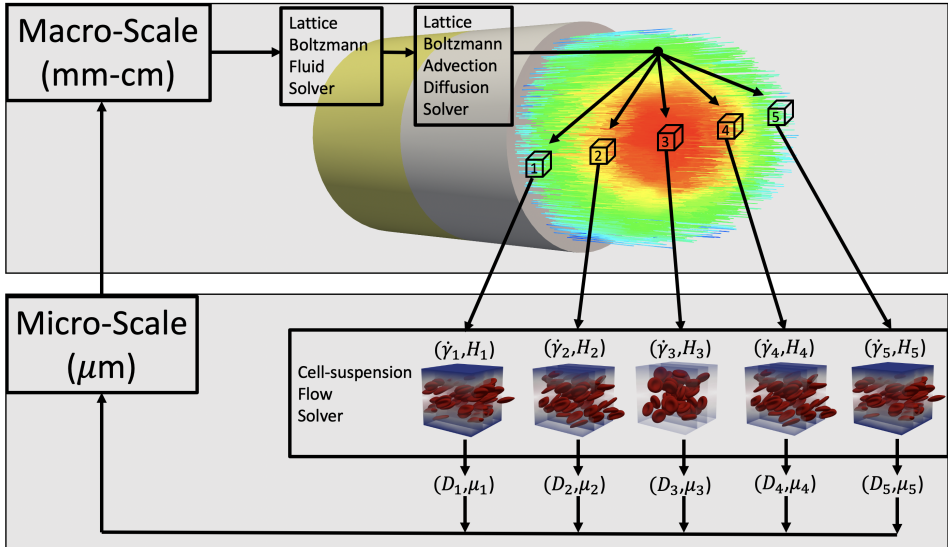


Figure 5.1: Schematic highlighting the physical scales and types of numerical models employed in the HMM model. The top panel shows the LBM advection diffusion solver for red blood cell concentration which is coupled to velocity field computed from a LBM flow solver. The bottom shows the cell-resolved micromodel simulation domains.

to improve the non-Newtonian models currently applied in complex tortuous geometries. Such contemporary non-Newtonian models are based on fits to data from simple shearing experiments or straight glass tube measurements. This HMM model could add more detail to the rheology in regions of special interest, such as the volumetric flow through a cerebral aneurysm, or even flow around micro-medical devices.

The general idea of the HMM model will be to solve blood flow as a continuum on the macroscale, and at each lattice location on the macroscale, spawn a micromodel cell-resolved simulation to model directly the motions of RBCs. The flow chart of the HMM model is given in Figure 5.2. Here numerical models operating on the macroscale are shown in red, models operating on the micro scale are shown in blue, intermediate model that could be deployed to increase computational performance are shown in green, data structures that are communicated between models are shown in white. Each sub-model operating on each scale will be described in complete detail in sections 5.3.1 and 5.3.2. A step by step iteration of the HMM model is first given to introduce the overall flow of the model and is as follows.

1. **Macro:** Iterate the LBM model to solve the fluid flow on the macroscale.
2. **Macro:** Pass flow field to LBM AD solver and iterate AD model to resolve the motion of RBCs on the macroscale.
3. **Macro:** Compute local shear rates and RBC concentrations at each lattice node on the macroscale.

4. **Communication:** Send local shear rates and hematocrits to the micro scale.
5. **Micro:** Simulate each shear rate and hematocrit combination on the micro scale.
6. **Micro:** Measure for each micromodel simulation a dynamic viscosity and RBC diffusion coefficient.
7. **Communication:** Send local viscosity and RBC diffusion coefficient to the macroscale.
8. **Macro:** Change the local viscosity at each lattice site as informed by the micromodel.
9. **Macro:** Change the local diffusion coefficient at each lattice site as informed by the micromodel.
10. Return to step 1.

This timestep routine is the most naive implementation of the HMM model. It is immediately clear that improvements can be made over the course of a simulation as there will be many repeated hematocrit and shear rate combinations, which results in repeated spawned micromodels that will impede computational performance. To alleviate such redundancies an intermediate model could exist between the macro and micro scales, increasing computational performance. Such a model could be as simple as an a priori function as a result from a fit of previous simulations, a intermediate database, or even a surrogate model [275] which can interpolate to return quantities from the micro scale without running the expensive micromodels. Such an intermediate model is conceptual in this current work, the implementation is left for future development. The general outline however, is illustrated here highlighting the locations where an intermediate model may be situated within the above routine and is shown as green boxes in Figure 5.2.

## 5.3. Methods

### 5.3.1. Macromodel

On the largest scales in this model blood flow is modeled as a continuous fluid using the lattice Boltzmann method (LBM) [78, 79]. This LBM solver will provide the overall flow and velocity field for the rest of the HMM model to be built upon. The Palabos framework [276] is chosen as the implementation to solve the computational fluid dynamics, specifically using the D3Q19 implementation [239], with the Bhatnagar-Gross-Cook (BGK) collision operator [95]. Since the cornerstone of the HMM model is the microscale cell-resolved models the development of the macroscale model begins with a conservative choice for the lattice resolution. Specifically, the lattice resolution on the macroscale will be equal to the size of an entire micromodel sub-domain. Therefore, the macroscale lattice is chosen with a spatial resolution of  $dx = 2 \times 10^{-5}$  m, with a time step of  $dt = 1 \times 10^{-5}$  s, a kinematic viscosity  $\eta = 1.1 \times 10^{-6}$  m<sup>2</sup>/s, a fluid density  $\rho = 1025$  kg/m<sup>3</sup>, which results in a relaxation time of  $\tau = 0.533$ . The choices of parameters are based on the validated parameters used for the fluid plasma used in HemoCell [15, 91, 119, 205].

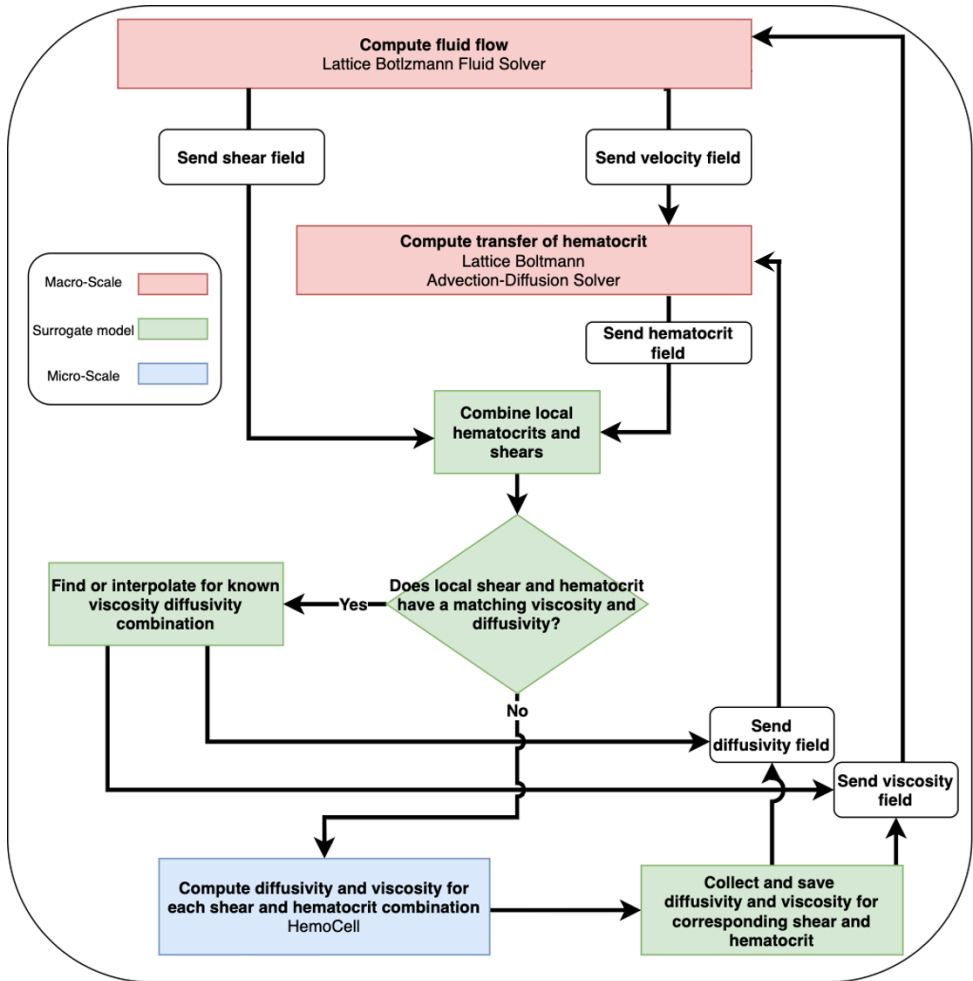


Figure 5.2: Workflow diagram of the HMM blood flow model. The Macro scale models are colored in red, the micro scale model is colored in blue, and the surrogate/interpolation model is colored in green. A demonstration of a similar framework with an implementation of a surrogate model has been carried out in [275].

The grid resolution on the macroscale may be eventually course grained to increase computational performance in larger vessel domains as demonstrated in previous work using BGK LBM [62, 231, 277]. The conservative choice in both spatial resolution of this model is for the purpose to first reach a benchmark physical validation before decreasing the spatial resolution and thus increase computational performance. Similarly the resolution in timestep, is chosen in order to properly capture the development of volume fraction profiles of cells which has been found to occur within 0.001 second [60].

The test simulations of the macromodel are performed under laminar flow conditions in an idealized periodic rectangular geometry. Flow conditions were chosen to match measurements of typical arteries with a diameters of 4 mm with a Reynolds number of 450 [278]. Fluid is driven via an external body force, the walls are defined with a no-slip boundary condition, which is implemented as bounce-back [97].

In addition to the LBM fluid solver which will describe the fluid flow on the macroscale, an advection diffusion solver is also used, coupled to the underlying fluid field, to track the motion of bulk RBCs on the macroscale. Given that the AD solver will have the same lattice resolution as the fluid solver, it will track the motions and transport of bulk RBCs over time. Just like fluid solvers, AD solvers come in two general varieties, namely Lagrangian and Eulerian. Previous Lagrangian methods have been used to solve the transport of particles (concentrations) using stochastic differential equations, which are consistent with the advection-diffusion equation [279–281]. When implementing a Lagrangian particle method, each particle will need to represent a collection of densities (in this case RBC concentration) which requires the use of a weighting function to map the actual macroscopic densities to the particles [282]. A recent HMM model for suspension flow has employed such a Lagrangian method for tracking concentrations of solid discs flowing in 2D, and was able to reproduce well known effects of shear thickening [281]. Eulerian methods for AD have documented limitations such as in the cases of large concentration gradients, and are susceptible to numerical dispersion and artificial oscillations [283]. Eulerian methods in particular have historically been limited to low Péclet numbers.

Recent improvements however have been developed to increase stability for simulations involving concentrations with high spatial variability [284] as well as those involving high Péclet numbers [285, 286]. This includes LBM methods that employ multiple relaxation parameters, such as the so called two-relaxation-time (TRT) [285, 287], and multi-relaxation-time (MRT) methods [288]. By introducing multiple diffusion (relaxation) parameters, in essence different time scales, increases stability as well as introducing computation time and implementation complexity.

The transport of cells in blood should be advection dominated, or strongly determined by the velocity of the flow field and therefore exhibit high Péclet numbers. This can inform the type of AD solver that will be suitable for tracking motions of continuum bulk RBCs in flow. Given the 4 mm diameter, Reynolds number of 450, and a typical diffusion coefficient of RBCs in whole blood, which are on the scale of  $\approx 1 \times 10^{-9}$  to  $1 \times 10^{-10}$   $\text{m}^2/\text{s}$  [289], we expect the system to be in the advection dominated regime for AD solvers. Grid Péclet numbers were calculated and shown in Figure 5.3, to highlight the range of Péclet numbers that the macromodel will encounter. The classical BGK LBM method used for AD has been shown to have a limit of a maximum grid Péclet number on the

order of  $\approx 1$  to 2 [290]. Therefore in this work an improvement on the single relaxation BGK LBM model is needed.

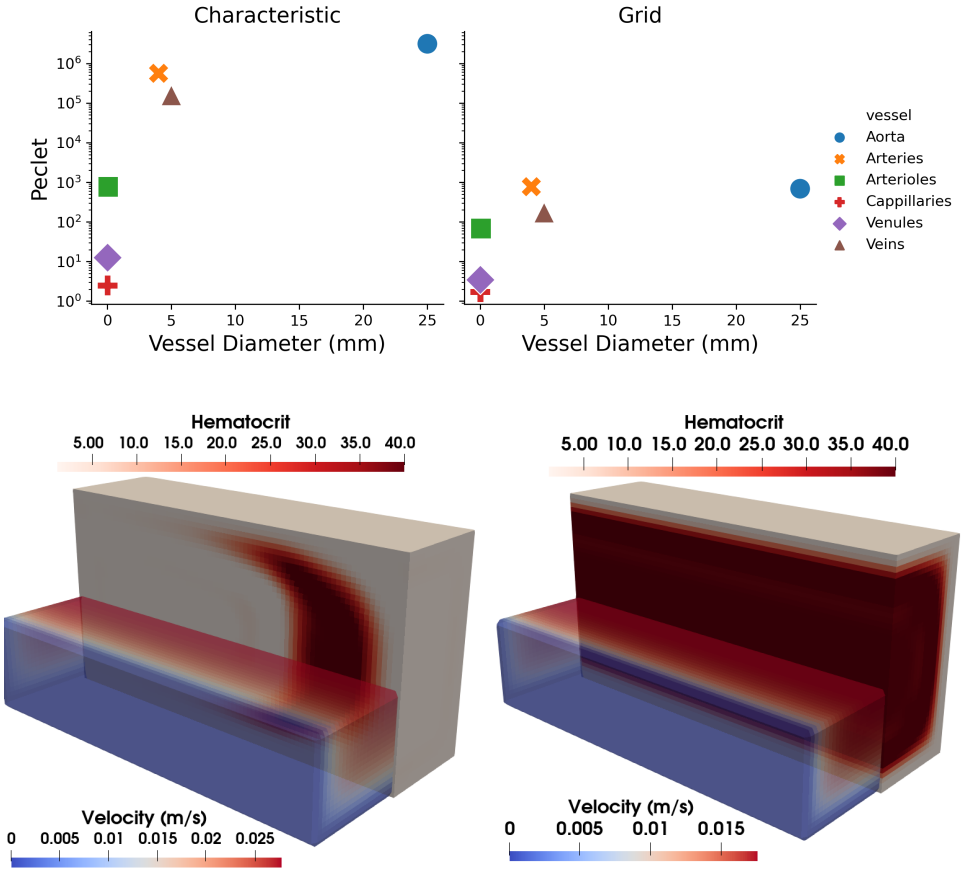


Figure 5.3: Top panel, typical Péclet numbers found in the human vasculature. The diffusion coefficient of RBCs in whole blood, was taken to be  $1.6 \times 10^{-9} \text{ m}^2/\text{s}$  [289], and flow velocities were taken from [278, 291]. Bottom left panel shows a snapshot of an initialized hematocrit slice, in a pure advected simulation. The bottom right panel shows a uniformly initialized rectangular channel with a hematocrit 40%, and RBC diffusion coefficient  $1.6 \times 10^{-9} \text{ m}^2/\text{s}$ .

Two recent improvements on the classical BGK LBM have been chosen as possible candidates for the AD solver on the macroscale. The first is a method that performs a regularization of the pre-collision distribution functions in terms of the local density, velocity, and momentum flux tensor [292–294]. The benefit of using such a regularization lattice Boltzmann method (RLB) is that it is not context-dependent, meaning that the relaxation parameter or parameters do not have to be chosen beforehand which are based on lattice velocities that will be present in any single simulation. The development and numerical validation of this method is elaborated in [292, 293]. The second applicable method is a single relaxation scheme used to solve high advection dominated transport

[284]. We test both methods following the simple advection tests laid out in a similar HMM model [281].

#### Advection Test

To ensure that the coupling on the macroscale can handle larger vessel sizes we set up two straight channel simulations mimicking millimeter sized arteries present in the body [278, 291]. The RLB AD solver [292, 293] is used. The diffusion coefficients for the RBC concentration fields are set to  $1.6 \times 10^{-9} \text{ m}^2/\text{s}$ , as suggested by recent measurements from diffusion-weighted MRI [289]. Neumann boundary conditions are imposed at the walls, that is the walls are set to a constant hematocrit of 0 and are isothermal as they are not allowed to “bleed” into the bulk flow concentrations in the channel. In the first simulation, the channel is initialized with a vertical strip of concentrated RBCs (hematocrit of 40%) in the channel. The diffusion coefficient of the AD solver is set to 0, enforcing the simulation to be completely advection dominated. The results of this simulation is shown in the bottom left panel of 5.3. The simulation is ran until the fluid reaches an equilibrium velocity ( $V_{max} = 0.3 \text{ m/s}$ ), where the initialized RBC concentration strip is advected with the fluid, and wraps around the domain. some numerical diffusion is observed which is a common problem for any LBM AD solvers. It should be noted that the rest of the domain is initialized to a hematocrit of 1, to not introduce unwanted numerical instability. The results of setting a zero hematocrit have not been tested in this study, but we do acknowledge that the including of other cell types which are sparse as compared to RBCs with volume fractions well below 1%. Such cell types are platelets and white blood cells would require the proper treatment of local concentration fields to be zero or close to zero. Another test of the coupling between the fluid field and the concentration field was performed, where the entire rectangular channel is initialized filled with 40% hematocrit, using the same Reynolds number and boundary conditions as slice case. The results of this simulation is shown in the bottom left panel of Figure 5.3. There are no numerical instabilities, in the form or oscillations or negative concentrations, observed in both simulations.

We also employ advection diffusion solver proposed by [284], which uses an additional reference relaxation parameter, as a sanity check for the RLB results. Since the system is in the advection dominated regime, we therefore pick a reference diffusion coefficient that is ten times greater then the diffusion of coefficient chosen for the concentration which is suggested by [287, 295]. With both solvers we observe no negative densities and no oscillations of either the LBM fluid, or the concentration field. This is observed for both initializations and for both AD solvers. Since the flow regimes achieved in the bottom two panels of Figure 5.3 exhibit high Péclet and Reynolds numbers, we deem both solvers effective for the scale of flow we wish to achieve in the first iteration of the HMM blood flow model. Though there exists numerical diffusion in these test simulations, we believe that updating the AD solver is a subject for future work. The flow regimes, of the aorta exhibit much higher Reynolds numbers, and can exhibit turbulence close to the heart, which is out of the scope for the types of problems and blood flow the HMM method is currently developed to achieve. For simplicity of a single relaxation parameter we then use the RLB AD solver proposed by [292, 293].

In the general time-step outline of the HMM model the macromodel will compute

both the flow field and the concentration field of whole blood and communicate the local shear rate and RBC concentration per lattice site to the micro scale. After an iteration of the micro scale, diffusion coefficients and viscosity per lattice node will be passed up from the micro scale, to be set on the macroscale. Efficient and physically correct results on the macroscale are dependent on the correct implementation and modeling performed on the micro scale.

### 5.3.2. Micromodel

The micro scale is modeled with the cell-resolved blood flow model HemoCell, in which plasma is modeled by the LBM, the mechanical model of the RBCs are described by a discrete element method and are couple to the plasma via the immersed boundary method [55, 91]. From each local hematocrit and shear rate combination on the macroscale, a cell-resolved micro scale will simulate perfect sheared environments using Lees-Edwards boundary conditions [296]. A single simulation will be spawned for each shear rate and hematocrit combination to solve for unknown RBC diffusion coefficients and dynamic viscosities.

Micromodel: Lees-Edwards boundary conditions within the cell-resolved lattice Boltzmann framework HemoCell

In order to compute the bulk viscosity and diffusivities from the cell-resolved model a uniform sheared environment is required. One common construction to induce a uniform shear environment is by implementing moving walls mimicking a parallel plate Couette viscometer. In such a set up a 3D domain is constructed with walls on two sides of the cubic domain, while the other walls remain periodic. By providing constant velocity to the parallel walls, one can induce an environment of uniform shear. This has one major caveat when including red blood cells in such a simulation domain, is that the walls affect the dynamics of RBCs close to the wall, namely the walls induce a lift force on the RBCs [49]. Among other phenomena the ability of the red blood cell to maintain a constant shape while under a constant shear (tank tread) induces a lift on the red blood cells [160]. Therefore, in bulk flow, RBCs on average migrate away from the walls creating a cell free layer [45, 297], and as a result a lubrication layer at the wall since the local viscosity in this region decreases and approaches that of the blood plasma in the absence of cells [20]. To alleviate the effect of walls on the computed viscosity of whole blood the domain can be made large enough that the walls do not affect the bulk flow properties. This however is not attractive as it will increase compute time, which negates the motivation of this chapter. A second option is to implement a wall-less simulation domain of uniform shear. These types of simulation domains were first developed by A.W. Lees and S.E. Edwards in 1972 [298] to study molecular dynamics in uniform shear flow.

Lees-Edwards boundary conditions (LEbc) are commonly used in molecular dynamics simulations as they allow the realization of a uniform sheared system without directly moving solid walls. Originally developed to study simple fluids underneath extreme conditions such as the transport properties of a fluid undergoing a shock wavefront. Lees-Edwards boundary conditions allow the examination of such extreme examples of transport processes. Here, simulations are periodic in all directions while also imposing con-

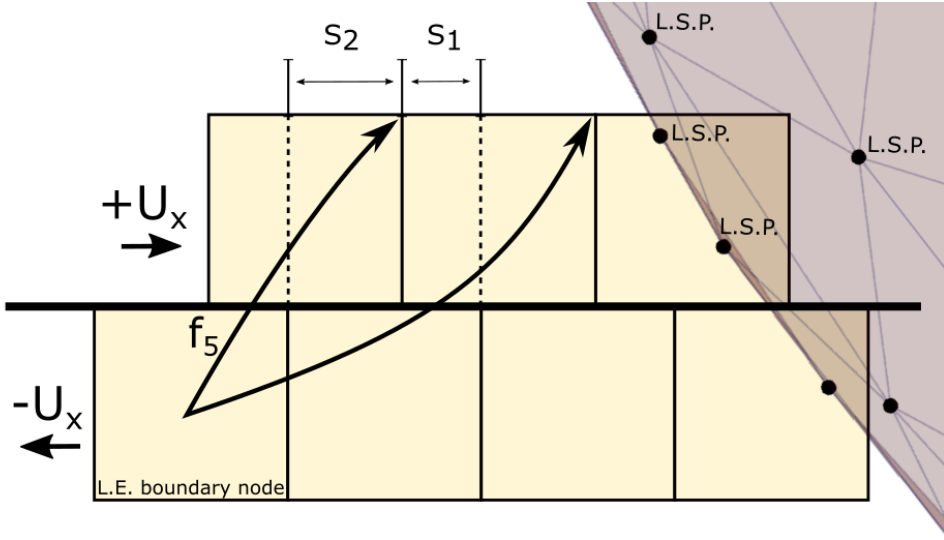


Figure 5.4: Schematic for a red blood cell crossing a Lees-Edwards boundary. Two rows of LBM nodes, which straddle the LEbc are shown in yellow showing the non-integer offset from one row of nodes to the virtual boundary. A small segment of an RBC is shown to highlight the size comparison between lattice nodes, RBC size, and LSP locations.

stant velocities on the two opposing periodic boundaries. The two boundary layers are prescribed a velocity of  $u_x = (-u_{LE})$  and  $u_x = (u_{LE})$  for instance. This will induce a uniform shear rate across for example the  $z$ -direction with a system height  $L_z$  of  $\dot{\gamma} = u_{LE}/L_z$ .

In Lattice Boltzmann simulations LEbc have been implemented for isothermal fluids [299] which has provided a practical solution to the problem of a maximum shear rate that is limited to less than  $1/L_z$  ( $L_z$  the transverse system size) in traditional lattice Boltzmann implementations of shear flow [300]. LEbc in the context of LBM has been extended to include systems with immersed particles as well. This includes LBM coupled with a finite element method describing deformable particles [301], as well as LBM coupled to spherical monodisperse population of particles [302–305]. The coupling schemes to resolve the interaction between the immersed boundaries of suspended particles and the LBM fluid vary from linear interpolation of the particle nodal velocities onto lattice distributions [301], to particle boundary conditions similar to bounce back boundary conditions [296, 302–304] which have been further developed to resolve sub-grid interactions [305]. In this work the immersed boundary scheme of [306] was used for the information exchange for the fluid-solid interaction between the immersed Lagrangian Surface Point (LSP) to the closest Eulerian points of the LBM fluid. The velocity is interpolated from the LSP onto the fluid, and the force is interpolated from the fluid onto the LSP. The implementation of LEbc described in [296] was followed. Here we set up domains which are periodic in all direction and solve the LBM equation over the entire domain

$$f_i(x + c_i \delta t, t + \delta t) = f_i(x, t) + \Omega_i(x, t). \quad (5.1)$$

This describes the density of particles  $f_i(x, t)$  that move with velocity  $c_i$ , in a direction  $i$ , to a neighboring point  $x + c_i \delta t$  over a time step  $t + \delta t$ . The collisions between particles are described through the commonly used BGK [95] collision operator  $\Omega_i$ .

$$\Omega_i(f) = -\frac{f_i - f_i^{eq}}{\tau} \delta t \quad (5.2)$$

The collision operator will relax the populations towards an equilibrium  $f_i^{eq}$  at a rate which is determined by the relaxation time  $\tau$ . The equilibrium distributions are given by

$$f_i^{eq}(x, t) = w_i \rho \left( 1 + \frac{u \cdot c_i}{c_s^2} + \frac{(u \cdot c_i)^2}{c_s^4} - \frac{u \cdot u}{2c_s^2} \right). \quad (5.3)$$

Here  $u$  is the velocity of the fluid and  $w_i$  are the weights specific to the chosen velocity set.

In addition to the LBM implementation the boundary LBM nodes on the top ( $z_{top}$ ) and bottom ( $z_{bottom}$ ) have an imposed macroscopic velocity during the LBM collision step. On the top boundary  $u_x = u_{LE}$  is prescribed as well as an equal but opposite velocity  $u_x = -u_{LE}$  is imposed on the bottom layer, which results in a uniform sheared environment. In order to correctly implement LEbc a Galilean transform has to be applied to the distributions traversing the  $+z/-z$  boundary. Here  $f_{i, \mathbf{u}_0}$  traverse the boundary to become  $f_{i, \mathbf{u}_0 \pm \mathbf{u}_{LE}}$  where  $\mathbf{u}_0$  denotes the reference velocity of the computational domain, and  $\mathbf{u}_{LE} = (u_{LE}, 0)$  denotes the velocity of the image system, which may not necessarily be an integer multiple of the lattice size. The shift in the densities that will stream over the boundary which is described by

$$f_{i, \mathbf{u}_0 + \mathbf{u}_{LE}} - f_{i, \mathbf{u}_0} \approx f_i^{eq}(\rho, \mathbf{u} + \mathbf{u}_{LE}) - f_i^{eq}(\rho, \mathbf{u}). \quad (5.4)$$

Where a Galilean transformation operator can be written following [296]

$$G_{\mathbf{u}_{LE}} f_i = f_i + f_i^{eq}(\rho, \mathbf{u} + \mathbf{u}_{LE}) - f_i^{eq}(\rho, \mathbf{u}) \quad (5.5)$$

from which then a propagation operator can be written

$$P_{LE} f_i((r)) = s_1 G_{\mathbf{u}_{LE}} f_i((r)_1 - \mathbf{e}_i) + s_2 G_{\mathbf{u}_{LE}} f_i((r)_2 - \mathbf{e}_i) \quad (5.6)$$

where the non-integer displacements can be accounted for, which are given by

$$\begin{aligned} s_1 &= \text{mod}(s_{LE}, 1), \\ s_2 &= 1 - \text{mod}(s_{LE}, 1), \\ \mathbf{r}_1 &= (x + \text{int}(s_{LE} + 1), y), \\ \mathbf{r}_2 &= (x + \text{int}(s_{LE}), y). \end{aligned} \quad (5.7)$$

It may be easier to see the application of LEbc in a simple spatial schematic, which is shown in 5.4. Two rows of LEbc nodes are shown, with the mapping of a LBM density  $f_5$  across the domain correcting for the displacement between the two nodes. Also shown in Figure 5.4 is the LSP points and a small section of an RBC in HemoCell.

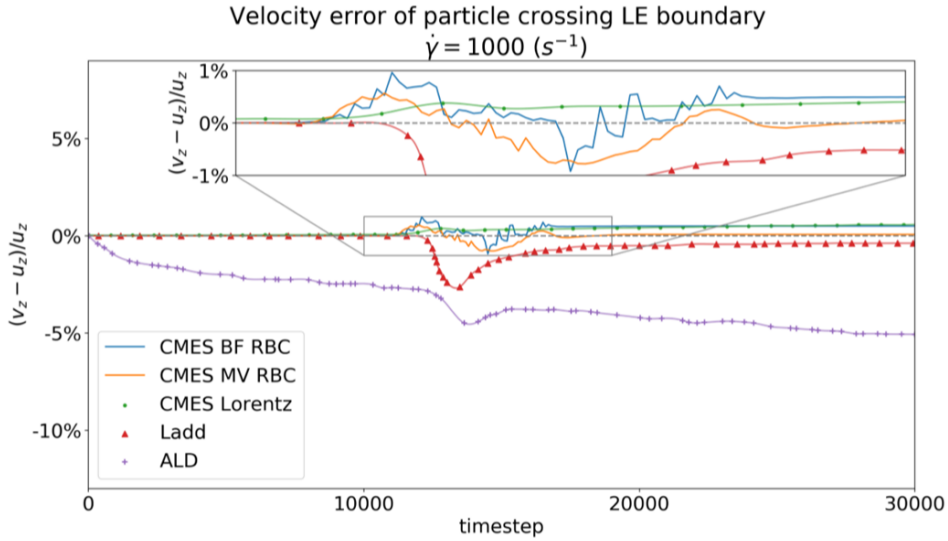


Figure 5.5: Prescribed velocity errors of a single RBC crossing a LEbc with a domain shear rate of  $1000 \text{ s}^{-1}$ . The results of a HemoCell RBC are shown in orange for the macroscopic velocity method and blue for a body force method. Green dots shows the results from Lorentz [296], red triangle show the results of Ladd [303], and purple crosses for ALD [307].

We implement two different methods of imposing a macroscopic velocity on the LEbc nodes. One is described above where we impose a macroscopic velocity (MV) when iterating through a collision step across the LE boundary nodes. The second method is by inducing a body force (BF) only on the boundary nodes, and was chosen as it was easier to implement in the LBM framework Palabos [276].

When a cell crosses the LE boundary it gets inserted on the other side of the domain. Here however, the new position also needs to be accounted for the displacement between image domains. Additionally, the velocity components of each LSP that make up the RBC need to be inverted in order to insert the particle with the correct momentum, matching the fluid environment. In previous studies including immersed particles, this is generally referred to corrected momentum exchange (CMES). Since each study involves different lattice spacing, particle type, and immersed boundary methods, usage of the term CMES can differ from study to study. Here CMES refers to the offset correction of the LSP position as it traverses the boundary as well as the inversion the LSP velocity.

The initial benchmark for a fluid-only LEbc simulations, we observe similar uniform shear rates across the domain as reported in [299], with a deviation from the expected shear profile of less than 0.01%. When including suspended particles with LEbc, a single RBC is placed in a sheared domain and prescribed a constant velocity and transverses the LEbc. We computed the percent error, and compare our implementation against those of Aidun, Lu, and Ding (ALD) [307–309], Ladd et al. (Ladd) [303, 304], and Lorentz [296]. The percent error in prescribed cell velocity  $v_z$  as it crosses the boundary is shown

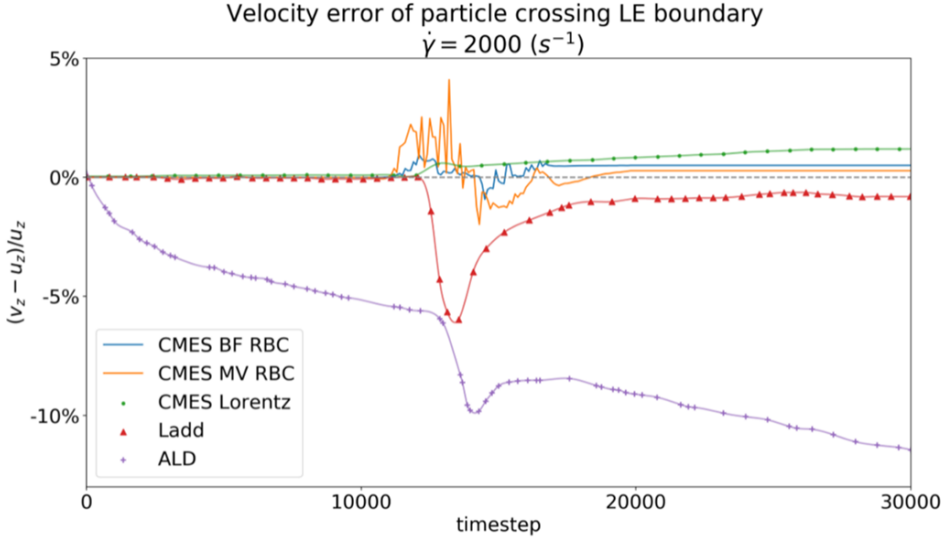


Figure 5.6: Prescribed velocity errors of a single RBC crossing a LEbc with a domain shear rate of  $2000 \text{ s}^{-1}$ . The results of a HemoCell RBC are shown in orange for the macroscopic velocity method and blue for a body force method. Green dots shows the results from Lorentz [296], red triangle show the results of Ladd [303], and purple crosses for ALD [307].

for two different shear rates,  $1000 \text{ s}^{-1}$  in Figure 5.5 and  $2000 \text{ s}^{-1}$  in Figure 5.6.

Our implementation compares well with existing implementations of LEbc with LBM and immersed particles. The velocity errors of a RBC as it crosses a LE boundary show better behavior than the implementation of Ladd and ALD, while performing similarly to Lorentz. This is observed in both the  $1000 \text{ s}^{-1}$  case and the  $2000 \text{ s}^{-1}$  case. The velocity error of our method in the  $2000 \text{ s}^{-1}$ , increases significantly compared to the slower shear rate case. It is however reassuring that in both cases very little transient velocity is introduced into the system as is especially the case with Ladd, and ALD. This is also evident, though less so, with the Lorentz implementation. The comparison of methods here may not be fully comprehensive as the immersed objects are different in each study. Lorentz[296] single LSPs represent rigid 2D discs, Ladd uses single LSPs for both 2D discs and 3D spheres[303, 304], where as ALD incorporates LSPs as deformable spheres [307–309]. Introduced errors will vary with choice of lattice resolution in relation to suspended object size. The relatively low errors in velocity of a suspended RBC crossing the LEbc in this study compared to the suspended objects crossing the LEbc in previous implementations, Figures 5.5 and 5.6, may be due to the large suspended RBC size to lattice spacing ratio. The size and number of LSPs comprising a single RBC in this study may lower the transient effect when an RBC traverses the LEbc. Highlighted in the schematic of Figure 5.4, is a small segment of a RBC traversing the LEbc.

## 5.4. Results

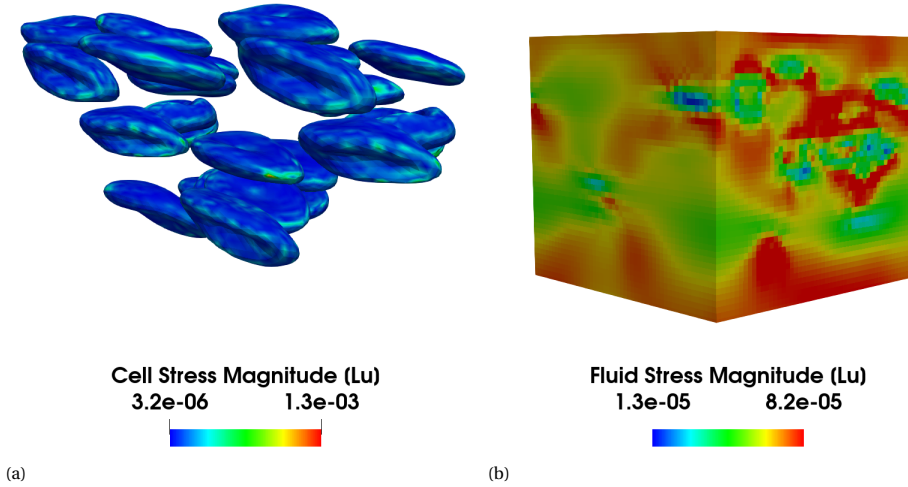


Figure 5.7: Stress patterns on the surface of the red blood cells in lattice units (left). Stress patterns computed from the underlying LBM fluid (right). Both panels are snapshots of the same simulation, but are shown apart to highlight each components contribution to the overall stress in the suspension.

#### Micromodel: Viscosity

The shear thinning effect in uniform shear environments was famously observed by Chien in 1966 [33]. This is primarily a consequence of the alignment and flattening of RBCs in flow [41, 42] reducing the collision frequency resulting in the decrease of the bulk viscosity [43].

The bulk viscosity arising from the cell-resolved simulations was computed following the simple definition of viscosity  $\mu = \frac{\tau}{\dot{\gamma}}$ . This requires the computation of the mean stresses present in the entire volume of a Lees-Edwards simulation. The mean stresses depend both on the stresses in the fluid  $\sigma_f$  and the stresses in the cells  $\sigma_{rbc}$ , at any given timestep i.e.  $\mu = \frac{\sigma_f + \sigma_{rbc}}{\dot{\gamma}}$ . The benefit of using LBM is that the fluid stress  $\sigma_f$  can be computed directly from the underlying fluid, previously shown in equation 3.1. The stresses from the cells can be computed from the mean stresses on the cell surfaces [310]. Since each RBC contains 642 LSP points the stresses on a single RBC are computed by mean from the stresses over all LSPs

$$\sigma_{rbc(i,j)} = \frac{1}{2N_{lsp}V_{rbc}} \sum_{n=0}^{N_{lsp}} (F_i x_j + F_j x_i). \quad (5.8)$$

Here  $V_{rbc}$  is the volume of the RBC approximated as  $90 \mu\text{m}^3$ ,  $F$  the tangential force at an LSP with a the position  $x$  with respect to the center of mass of the RBC. The subscripts  $i$  and  $j$  denotes the directions of the components of the force and position vectors respectively. Each of the stresses are visualized in Figure 5.7b, with the stresses on the RBCs shown in the left panel and the fluid stresses shown in the right panel.

Average dynamic viscosity was computed at 10 separate time points after each sim-

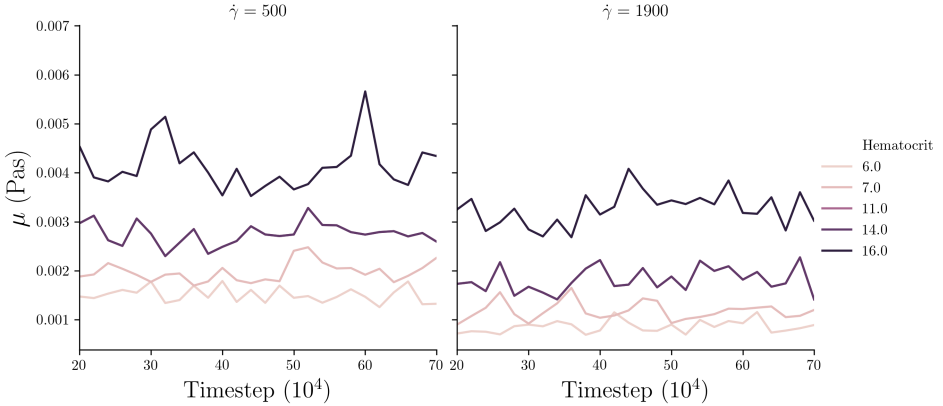


Figure 5.8: The time series of computed dynamic viscosity in LEbc simulations over a range of hematocrits. Two shear rate cases are highlighted, a shear rate of  $500 \text{ s}^{-1}$  (left panel) and  $1900 \text{ s}^{-1}$  (right panel).

ulation reached an equilibrium shear rate. The equilibrium shear rate was identified to occur in all simulations after a strain rate of  $\tau \approx 2$ . Computed viscosities are shown over time for two separate shear rates with varying hematocrits in Figure 5.8. Lower hematocrit cases reached an equilibrium shear rate sooner compared to the higher hematocrit cases. The higher hematocrit cases additionally has a higher variance in viscosity values, since the domain size is smaller with respect to the number of cells present in the domain. If the size of the simulation domain were increased, it should be expected that the variance of viscosity values would decrease, as the individual cell motions will not influence the overall measurement.

To confirm the results of each micromodel simulation, the computed viscosities over multiple shear rate and hematocrit combinations are compared to experimental values. The results are shown in Figure 5.9. Here initializations from 32% to 10% hematocrit case were simulated over 5 shear rates ranging from  $100$  to  $1000 \text{ s}^{-1}$ . The results highlight shear thinning behavior for each hematocrit initialization. The data from [13], plotted in black in Figure 5.9, highlights the experimental evidence of the shear thinning effects of whole blood at three different hematocrits. The data sets of Chien [13], and the numerical results from HemoCell, also exhibit an increase in viscosity across all shear rates when hematocrit is increased. We anticipate that the increase in the hematocrit results in more RBCs present, and thus more collisions which introduce more stresses into the surrounding fluid. By increasing the number of RBCs in essence absorbs more momentum from the blood plasma and effectively increases the overall bulk viscosity.

It should be noted that there is no cell-cell interaction or lubrication implemented in HemoCell and is likely limited to only properly model suspension behavior for shear rates above  $\approx 10 \text{ s}^{-1}$ . Healthy RBC membranes generally contain an overall negative electric charge, referred to as the zeta potential [312, 313], which provides a repulsion between two RBCs. This repulsion can be broken down in the presence of positively charged plasma proteins [314], which diminishes the electric repulsion between two RBCs, and even allow RBCs to form rouloux [315]. The formation of rouloux structures

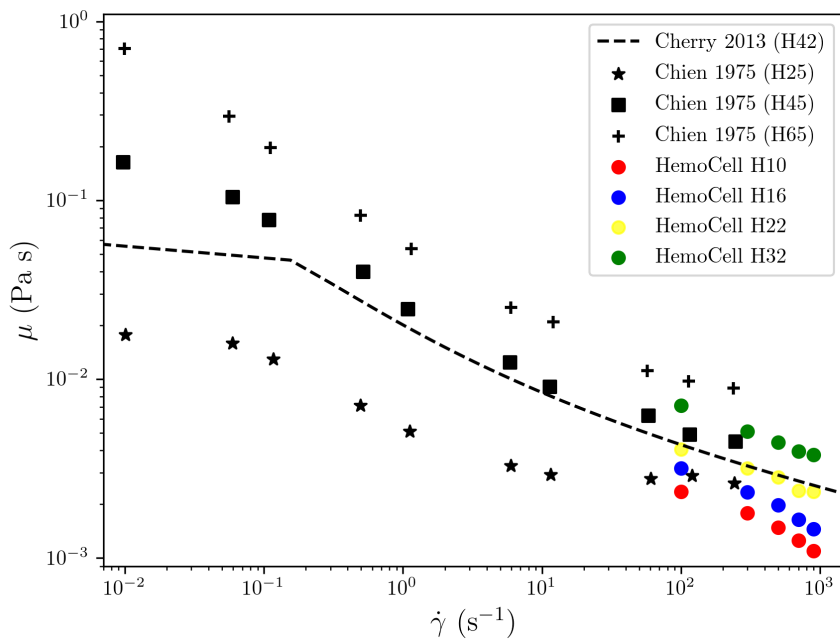


Figure 5.9: The experimental Chien data [13] for multiple hematocrits are shown with black stars for 25%, squares for 45% and crosses for 65%. HemoCell results are shown as circles green for 32%, yellow for 22%, blue for 16%, and red for 10% hematocrit. The numerical fit from Cherry et al [311] for 42% hematocrit is shown as a dashed line.

[37–39] at shear rates lower than  $10 \text{ s}^{-1}$ , is one of the main contributions to the viscoelastic behavior of whole blood [34, 35]. HemoCell does exhibit rouleaux formation but does exhibit shear-thinning. The correct implementation of a zeta potential in HemoCell may be needed to properly model blood flow below shear rates of  $10 \text{ s}^{-1}$ .

#### Micromodel: Diffusion

Using the proposed LEbc in this chapter to calculate cell diffusion coefficients can mitigate limitations in present in previous numerical studies such as wall effects [316], idealized geometries [60], and 2D effects [59]. The diffusion of RBCs in blood flow is in large part influenced by the local shear rate. And in accordance, the shear induced diffusion of RBCs has widely been employed with linear scaling in course-grained numerical blood flow models [317–319]. Recent cell-based numerical work, however, has identified a departure from linear scaling of shear induced diffusion [59, 316]. And most recently further also identified that RBC diffusion and platelet margination is also depends on gradients in hematocrit [60] in addition to shear rate.

The diffusive behavior of cells was extracted from a finite time domain, referred to as time-window, of  $\tau = 3[\dot{\gamma}t]$ , and is consistent with previous works [60, 119]. Shown in Figure 5.10, are the computed diffusion coefficients per time-window  $\tau$  of red blood cells along the velocity gradient direction of three LEbc simulations with varying shear rates. In Figure 5.10 the diffusive regime can be identified in the time-windows of  $\tau = (0.0015, 0.002, 0.006, 0.03) \text{ s}$  for the respective shear rates  $\dot{\gamma} = (1900, 1500, 500, 100) \text{ s}^{-1}$ .

#### Micromodel: Final Results

The resulting computed viscosities and diffusion coefficients from an array of simulations ranging from shear rates of 100 to 2000  $\text{s}^{-1}$ , and hematocrits ranging from 6% to 32% are summarized in Figure 5.11. The left panel of Figure 5.11 shows the computed dynamic viscosities and the right panel shows the diffusion coefficients, all data points from simulations are shown as black dots. An estimation can be made for the topology of these two phase spaces by performing a simple least squares fitting of a 2D polynomial to the simulation data. The fit to the data highlights a relationship that is a 2nd order 2D polynomial for dynamic viscosity, and a linear relationship for the diffusivities of RBCs. The resulting fitted functions are shown as 3D planes, in Figure 5.11. The least-squares solution found for the dynamic viscosity data can be written as

$$f_{\eta}(\dot{\gamma}, H) = c_0 + c_1\dot{\gamma} + c_2H + c_3\dot{\gamma}^2 + c_4\dot{\gamma}^2H + c_5\dot{\gamma}^2H^2 + c_6H^2 + c_7\dot{\gamma}H^2 + c_8\dot{\gamma}H. \quad (5.9)$$

And the least-squares solution found for the diffusion coefficient data can be written as

$$f_D(\dot{\gamma}, H) = c_0 + c_1\dot{\gamma} + c_2H + c_3\dot{\gamma}H. \quad (5.10)$$

The coefficients for each polynomial are reported in table 5.1.

The non-linear relationship of viscosity with respect to shear rate should be recognizable as it is predicted by Chien [13]. However there has been no experimentally determined relationship of whole blood viscosity for both shear and hematocrit together. The

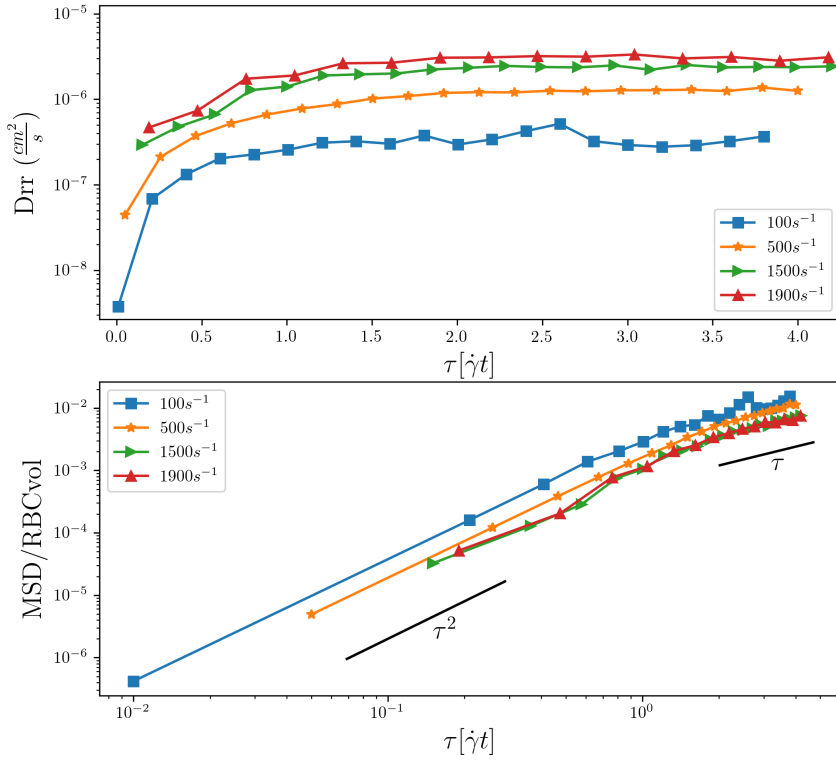


Figure 5.10: The top panel shows diffusion coefficients as a function of time-window  $\tau$ . The bottom panel shows computed mean squared displacement (MSD) of RBCs in the velocity gradient direction. The ballistic regime is observed in section of the MSD curve with a slope of 2, and the diffusive regime is observed in the section with a slope of 1.

Table 5.1: Coefficients for least squares fit to micromodel output.

Polynomial Coefficients		
Coefficient	$f_{\eta}$	$f_D$
$c_0$	3.02	1.31e-8
$c_1$	-3.83e-3	2.89e-10
$c_2$	1.09e-6	1.99e-8
$c_3$	-2.13e-1	-7.94e-12
$c_4$	7.84e-4	
$c_5$	-2.94e-7	
$c_6$	3.18e-2	
$c_7$	-4.70e-5	
$c_8$	1.59e-8	

unknown relationship of viscosity as a function of hematocrit in the phase space of Figure 5.1 indicates that the least squares fitting may not be the best method to determine the topology. Which is also suggested by a higher sum of squared residuals, reported as 13.9, resulting from the viscosity fit. The diffusion coefficients in the right panel of Figure 5.1 however show a linear relationship with both hematocrit and shear rate. The sum of squared residuals from the least squares fit to the diffusivities is much lower, at a value of  $4.4 \times 10^{-13}$ . Further analysis of this phase space is needed to accurately report the relationship of diffusion and bulk viscosity as functions of hematocrit and shear. The number of micromodel simulations shown here are only performed once, per shear rate and hematocrit combination. Increased resolution along with multiple simulations per shear and hematocrit pair are needed to provide more robust statistics in order for such a topology to be determined.

### Macroscale

Once the solutions are known on the microscale the quantities are then communicated back up to the macroscale lattices. The local viscosities and diffusivities are imposed on the macroscale by setting the local relaxation parameters on each LBM node for both fluid and concentration lattices. Four separate simulations were carried out using the HMM model, with varying rectangular channel widths of 0.1, 0.2, 0.3 and 4 mm. The resulting hematocrit, velocity, and shear rate profiles for each simulation are reported in Figure 5.12. An increase of shear rates is observed as channel width decreases, which is expected as the velocity profiles on the smaller scales become less blunted and more parabolic. The hematocrit profiles however show a concentration peak in the center for the smallest channel widths. The concentration peak then moves progressively towards the vessel wall as channel width increases. This suggests that the current setting of the local relaxation parameters may not be implemented correctly since the behavior observed in the concentration profiles is expected if the concentration profiles are only influenced by the underlying fluid field. When the concentrations peak on the macroscale we expect an increase in the local diffusivities as well, which would lead to a flattening out of the hematocrit profile. Additionally increased bluntness of the velocity profiles is not observed with decreasing channel width. This should be expected as higher concentrations of RBCs in the center should lead to a dampening of the velocity profiles at similar locations. The increased presence of RBCs should therefore increase the local viscosity in those regions [54, 91].

To estimate the number of repeated hematocrit-shear rate combinations that will occur on the macroscale for a preliminary HMM run, a simple data base is implemented. The database stores computed viscosities and diffusivities per hematocrit and shear rate combination to alleviate repeated micromodel simulations. Shown in Figure 5.13 are data base entries on the macroscale, as the flow and concentration fields develop from initialization. The results shown in Figure 5.13, are from the 0.2 mm HMM run, which was initialized uniformly to a hematocrit of 40 % and flow was initially zero. The database is queried every 600 timesteps from start up till the system has reached a steady state. The build up of the flow field can be observed in the first three panels of the times series, when the system seems to have reached a flow equilibrium by the 3000 timestep, which corresponds to a physical time of 0.003 seconds. Additional database entries are made

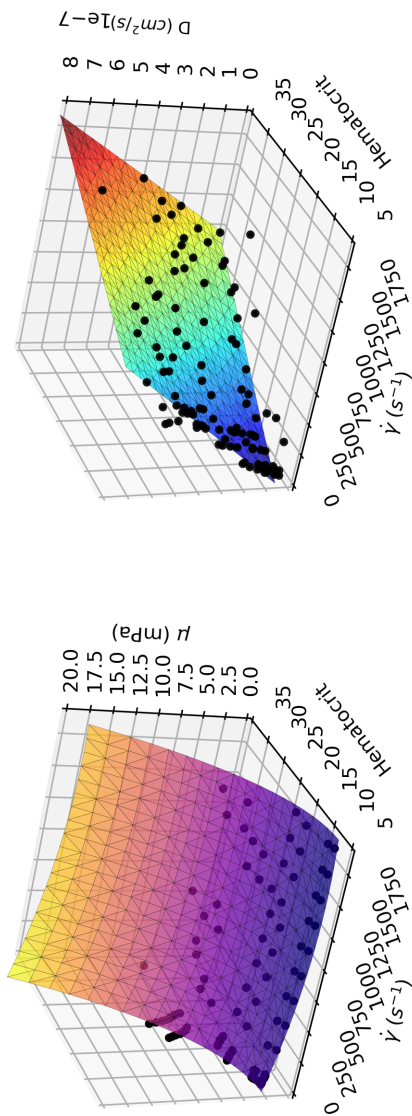


Figure 5.11: Left panel shows the computed dynamics viscosity from a range of LEbc simulation across multiple hematocrit and shear rates. The left panel shows the computed diffusion coefficients from the same LEbc simulations.

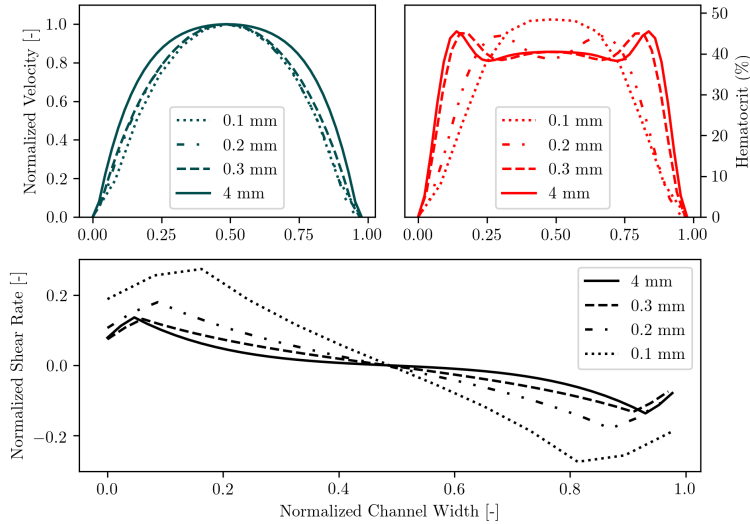


Figure 5.12: Velocity, hematocrit, and shear rate profiles on the macroscale of the HMM blood flow model. The HMM simulations were performed in periodic rectangular geometries, with channel widths of 0.1, 0.2, 0.3, and 4mm respectively. Each HMM run was initialized to 40% hematocrit.

after the system reaches flow equilibrium, as we expect the concentration fields are not yet in equilibrium.

## 5.5. Discussion

The initial development and implementation of an HMM model for blood flow is presented. The focus of this model is to correctly describe the viscosity and RBC diffusion on scales that are currently unachievable by contemporary cell-resolved blood flow models. The model operates on two scales, a macroscale where continuum LBM solvers are used, and a microscale where cell-resolved model is used. It was determined that the usage of the classical BGK LBM to describe the fluid field is sufficient to model blood flow in vessel of at least 4mm in diameter. A regularized LBM solver [292, 293] is used as an AD solver to describe the motions of rbc concentrations on the macroscale. It was determined that the regularized LBM method presented no numerical instabilities or oscillations. On the microscale, Lees Edwards boundary conditions were developed to properly simulate uniform sheared experiments for the cell-resolved blood flow model HemoCell. The viscosity curves of Chien [13, 33, 43] were matched as a result. A relationship with shear rate and hematocrit was determined for both viscosity and RBC diffusion. Finally, multiple HMM runs were performed in rectangular channels with varying channel widths. The HMM runs suggest that such a model can be employed to solve blood flow in vessels currently too large to solve with cell-resolved blood flow models. Further development is needed to ensure the local relaxation parameters on the macroscale are being

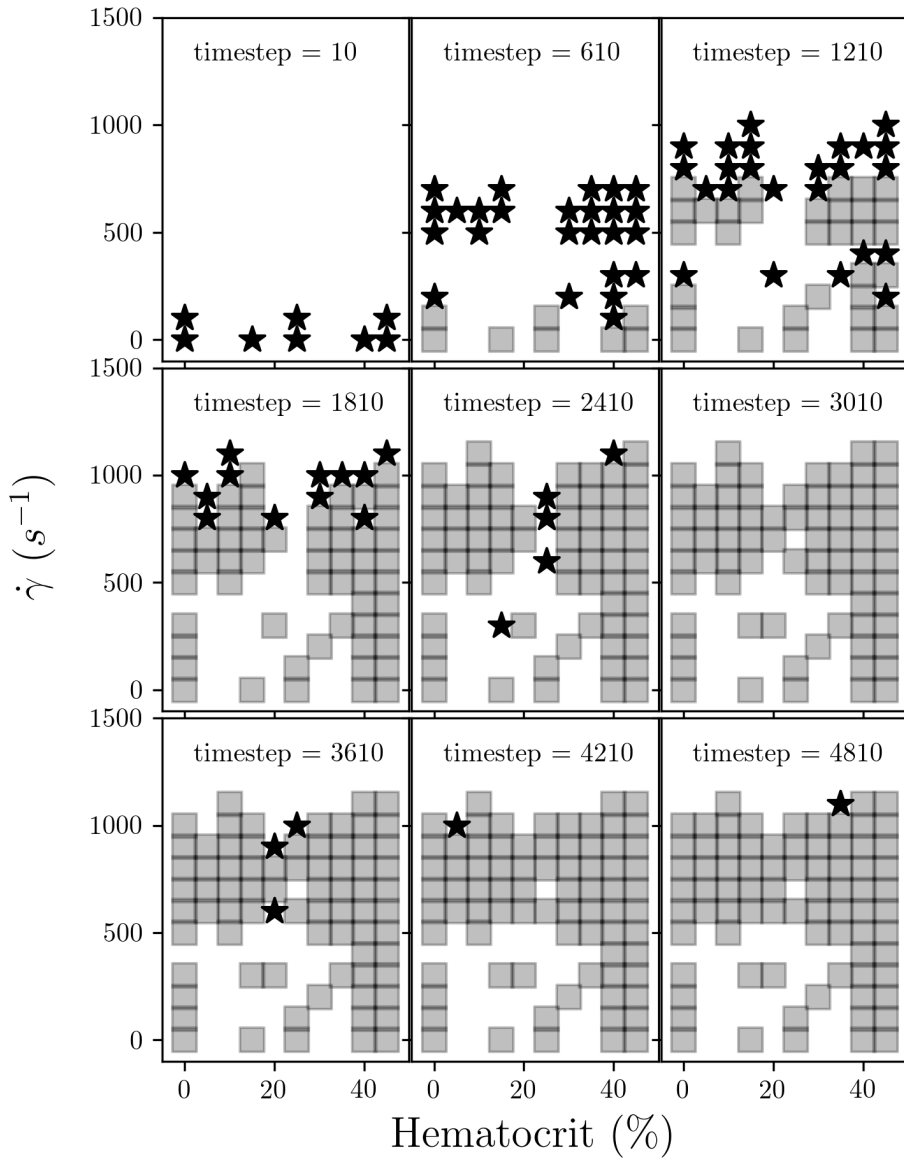


Figure 5.13: Data base entries for the HMM model run in a rectangular channel with a 0.2mm channel width at 40% hematocrit. New entries into the data base are shown as black stars, and existing entries are shown as grey squares. Each panel shows snapshots over time of the state of the database.

set correctly, to properly recover the non-Newtonian behavior of whole blood on the macroscale.

The novelty of developing an HMM model for blood flow is that it can be extended to include models that are not limited to only modeling fluid dynamics. Given the heterogeneous nature of this model, computational models which include the formation of a platelet aggregate to model the formation of a blood clot [273], brain blood flow and perfusion, stent deployment models [67], in stent restenosis models [62] for example, can also be included to contribute to a more complete HMM model for the virtual physiological human.

A more specific application of the HMM blood flow model could be to incorporate vessel geometries. A sample vessel domain on the macroscale could be decomposed into multiple cell-resolved simulations, with varying boundary conditions. In addition to the existing LEbc, which would be performed for regions away from the vessel walls, additional micromodels with a single moving wall need to be included in order to capture the interaction of whole blood with the vessel walls. This would be implemented on the microscale by providing a constant velocity on a single bounce-back wall which in turn will provide a uniform shear in the domain. Cells in this simulation setup would additionally interact with the presence of the wall. Validation of the HMM model with the presence of wall would need to be carried out reproduce known phenomena such as the Fåhræus-Lindqvist effect.

It is an open question of how many sub-simulations are needed to correctly resolve the known properties of whole blood, like the Fåhræus and Lindqvist effect, the cell free layer, and shear thinning on the macroscale. When the macroscale model is solved, the appropriate micromodel resolution must be chosen need to be in order to maintain accurate physical behavior on the macroscale. This type of spatial course-graining of the micromodels, so called gap tooth methods [320, 321], have proven successful, and given the choice of lattice spacing on the macroscale is a promising method for decreasing computational overhead. Another issue that needs to be addressed is largest each micromodel simulation domain needs to be to accurately resolve the local viscosity  $\eta_i(x_i, H, \dot{\gamma})$  and diffusion coefficients  $D_i(x_i, H, \dot{\gamma})$  to be returned to the macromodel. Sensitivity analysis therefore should be performed on the microscale domain size, and its relation to returning a repeatable quantity. In terms of computational performance we are motivated to make the micromodel domains as small as possible.

### 5.5.1. Coupling Between Microscale and Macroscale

To avoid duplicate micromodel simulations for repeated shear rate and hematocrit combinations the implementation of an intermediate database between the macro and micromodel could reduce the computational overhead of the proposed HMM. In addition viscosities could be interpolated from a surrogate model which would sample and interpolate (based on a Gaussian process for example) from known values from the database to return a reasonable viscosity or a diffusion coefficient without running a micromodel. If there are missing viscosities and/or diffusion coefficients then a micromodel will be spawned for each unknown shear rate and hematocrit combination.

Communication between models also needs to be developed. Currently shear rate, diffusion, and viscosity data is communicated between models via input and output of

---

files. This causes a significant I/O bottleneck and can be resolved through the use of a multiscale coupling library [322], where the separate models are linked and data is exchanged over the network in a peer-to-peer fashion. Furthermore multiscale applications, such as the one in proposed in this chapter, can be developed to run at the exascale. Heterogeneous multiscale computing techniques are being developed to handle internal queuing and multiple sub-model execution on large-scale supercomputers, together with a data-informed execution time prediction model [275].